Analyst

Accepted Manuscript

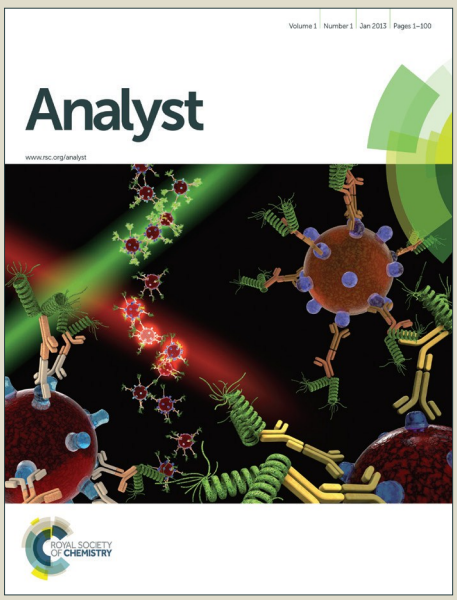

ROYAL SOCIETY OF CHEMISTRY

www.rsc.org/analyst

For submission to
Analyst

A Simple Integrated Microfluidic Device for the Multiplexed Fluorescence-free Detection of *Salmonella enterica*

Briony C. Strachan[1±], Hillary S. Sloane[1±], Eric Houpt[2], Jacob C. Lee[1], Daniel C. Miranian[1], Daniel A. Nelson[1] and James P. Landers[1,3,4*]

[1]Dept of Chemistry, McCormick Road, University of Virginia, Charlottesville, VA 22904
[2]Dept of Infectious Disease, University of Virginia Health Science Center, Charlottesville, VA 22908
[3]Dept of Pathology, University of Virginia Health Science Center, Charlottesville, VA 22908
[3]Dept of Mechanical Engineering, University of Virginia, Engineer's Way, Charlottesville, VA 22904

Keywords: Integration, hybridization, PCR, fluidic control

± Authors contributed equally to this work

*To whom correspondence should be addressed:
Prof. James Landers
Department of Chemistry
University of Virginia
McCormick Road
P.O. Box 400319
Charlottesville, VA 22904
Ph 434-243-8658
Fx 434-243-8852
E-mail: landers@virginia.edu

Abstract

Rapid, inexpensive and simplistic nucleic acid testing (NAT) is pivotal in delivering biotechnology solutions at the point of care (POC). We present a poly(methylmethacrylate) (PMMA) microdevice where on-board infrared-mediated PCR amplification is seamlessly integrated with a particle-based, visual DNA detection for specific detection of bacterial targets in less than 35 minutes. Fluidic control is achieved using a capillary burst valve laser-ablated in novel manner to confine the PCR reagents to a chamber during thermal cycling, and a manual torque-actuated pressure system to mobilize the fluid from the PCR chamber to the detection reservoir containing oligonucleotide-adducted magnetic particles. Interaction of amplified products specific to the target organism with the beads in a rotating magnetic field allows for near instantaneous (<30 sec) detection based on hybridization-induced aggregation (HIA) of the particles and simple optical analysis. The integration of PCR with this rapid, sequence-specific DNA detection method on a single microdevice presents the possibility of creating POC NAT systems that are low cost, easy to use, and involve minimal external hardware.

Introduction

The sensitive and specific identification of nucleic acid targets is central to the fields of clinical diagnostics, food safety, forensics and environmental microbiology. Nucleic acid testing (NAT) typically incorporates amplification and detection technologies, many of which require complex operational steps and expensive instrumentation[1, 2]. Such resource-intensive processes limit the use of NAT assays to reasonably skilled personnel in centralized laboratories and presents challenges for its use at the point-of-care (POC). However, important applications, such as pathogen detection in remote environments and time-critical diagnostics, require assays that can be performed in POC settings[3, 4]. The profound impact promised by microfluidics has garnered extensive efforts focused on the development of truly portable POC NAT technologies[1, 5, 6], and many of these involve the incorporation of amplification and detection strategies onto a microfluidic platform[7]. Microfluidic assays offer the advantages of rapid analysis, low power consumption, and functional integration of multiple analytical processes[8]. By exploiting the strengths of microfluidics, microdevice-based NAT technologies have the potential to be low cost, portable, and easy-to-use, which are qualities that are critical for implementation at POC.

Some form of amplification is almost always required in NAT to provide specificity, increase the signal, and assure detection of a specific target. A number of techniques have evolved, including strand-displacement amplification[9], nucleic acid sequence based amplification[10], and rolling-circle amplification[11], but polymerase chain reaction (PCR) remains the most popular due to its simplicity and amplification power[12]. PCR on a microfluidic device was first demonstrated in 1993, and has since been replicated and improved in a number of formats[13, 14]. Our group has successfully demonstrated noncontact infrared (IR)-mediated PCR (IR-PCR) for chip-based

amplification, and shown the capabilities of this platform to be multiplexed, as well as integrated with upstream and downstream analytical processes[15-17].

The post-amplification analysis of DNA takes on multiple forms for end-point or real-time detection, and these range from hybridization microarrays to capillary electrophoresis and capillary gel electrophoresis, among others[1, 12, 18-23]. Despite the successful implementation of these detection methods on microdevices, many are unsuitable for implementation on POC platforms as a result of the expensive and complex instrumentation required. An attractive detection approach would involve minimal peripheral instrumentation and provide a simple output for interpretation. As such, visual detection methods are an attractive tool for POC applications[4].

We recently reported a novel particle-driven technique for the visual detection of DNA targets on a microfluidic platform, termed hybridization-induced aggregation (HIA)[24, 25]. HIA utilizes a pair of oligonucleotide probes that are complementary to the target DNA sequence. The probes are immobilized on the surface of paramagnetic particles (via biotin-streptavidin conjugation), and their interaction with target DNA is enhanced by a rotating magnetic field (RMF). The hybridization of the target sequence to the particle-bound probes induces aggregation of the particles in a manner that rapidly provides visual confirmation of the presence of target DNA in the sample. Core to the power of HIA is the ability to differentiate target-specific amplicons from non-specific nucleic acid sequences, which, coupled with the specificity of PCR amplification, brings a second level of specificity to the assay. The inherent simplicity and specificity of HIA make it an ideal approach for end-point detection on a NAT device.

A significant challenge facing the integration of amplification and detection processes are related to microfluidic control and device operation[5]. Necessary fluid handling and actuation almost always requires the use of complex and bulky peripherals that are not amenable to POC testing. Human operated fluid pumps, such as finger pumps[26-28], have emerged as attractive techniques for fluid actuation in microfluidic systems that can be considered portable. In the current work, we exploit a small machine screw to facilitate fluid movement in our microdevice, which is hand-operated and does not require additional equipment or resources. The torque-actuated pressure (TAP) provided by the screw provides deflection of an elastomeric material into a fluid compartment, which displaces the fluid and drives it into a microchannel. In a similar approach, Weibel et al. previously demonstrated the use of screws embedded in a PDMS microdevice ('TWIST valves') for fluid pumping[29]. The TWIST valves create compartments in which fluids are held under pressure. Upon opening the TWIST valves, the pressure, stored in the elastic deformation of the walls and ceiling of the PDMS, pushes the fluid out of the compartments and into microfluidic channels.

It is imperative to control the actuation and timing of fluid flow in integrated microfluidic devices. This has traditionally been achieved with pneumatic valves[30] that require external hardware (e.g., vacuum pumps or electronic junctions)[31], escalating the cost and footprint of the micro-platform. Geometric passive valves are attractive because they exploit the microchannel architecture itself to create surface tension at the meniscus that halts fluid flow via capillary action. Such passive valves have been challenging to create in PMMA, an increasingly common material in microdevice fabrication due to low cost and rapid fabrication with CO_2 laser ablation. The difficulty in creating passive valves in PMMA is due to roughness of the surface and lack of precision associated with laser ablation-based microfabrication. Recently, Mohammed et al.

described "rastering" the PMMA surface (many low power laser passes over the surface) to create a 600 μm deep geometric burst valve in PMMA[32]. PMMA capillary burst valves have also been shown in a centrifugally-driven microfluidic device with channel depths of 500 μm using CNC-assisted micromilling[33] . Both processes create wide, deep channels that are more likely to collapse during bonding, while also increasing reagent waste/loss. As a result, a "vector cut" (a single high-powered pass of the laser over the PMMA surface) is preferable, as it is capable of generating shallow, narrow channels. In this report, we demonstrate a novel passive geometric burst valve created in PMMA with a vector cut, circumventing the issues seen with previous efforts.

Achieving fluidic control with a novel laser-ablated capillary burst valve and manual torque-actuated pressure system allowed for the integration of multi-sample IR-PCR with HIA-based detection on a simplistic PMMA microdevice (**Fig. 1**) . We demonstrate the utility of this device for the rapid detection of the zoonotic pathogen *Salmonella enterica* [34], an organism of substantial public health concern.

Experimental

Microdevice design

Four ellipsoid PCR chambers (5 mm long, 1.25 mm wide, 0.5 mm deep) are symmetrically oriented within the 7 mm (diameter) focal spot of the halogen lamp for IR-PCR to allow even heating across all chambers. Three of the PCR chambers are each connected to a separate TAP inlet (2.66 mm diameter, 1 mm deep) and HIA detection chamber (5 mm diameter, 1 mm deep). Along each of the channels connecting the PCR and HIA chambers (14 mm long, 150 μm wide, 170 μm deep), there are two adjacent oval-shaped capillary burst valves (170 μm deep). Though only one valve is functionally necessary, an additional valve is added to account for any fabrication failure in the first valve. The channels are designed such that the HIA chambers are vertically aligned. Additional features (or "air pockets") surrounding the primary architecture of the microdevice were created to reduce the thermal mass of the device and to aid in bonding during device fabrication.

Fabrication of the microdevice, manifold, and rotating magnetic field construct

The microdevice architecture was designed using AutoCAD software. A VersaLASER system 3.50 from Universal Laser Systems (Scottsdale, AZ) was used to ablate the architecture into PMMA (0.5mm thick) purchased from Astra Products (Baldwin, NY) for each of the three layers of the microdevice. The layers were then thermally bonded using established methods, to create a microdevice with a total thickness of 1.5 mm [35]. After loading the PCR reagents into the device, the device was sealed with MicroAmp® qPCR adhesive film from Applied Biosystems (Grand Island, NY). A manifold was constructed using 2 layers of PMMA (each with a thickness of 0.635 cm), which encased the microdevice while keeping the PCR and HIA

chambers uncovered (see Figure 6). A septum (PTFE face/silicone body) from Sigma Aldrich (St. Louis, MO) was placed above each of the three sample inlets, between the microdevice and the top layer of the manifold. 6-32" mechanical screws were incorporated into the top layer of the manifold, with one above each of the three sample inlets. 3 additional mechanical screws were used to "close" the manifold and pressurize the microdevice.

The rotating magnetic field construct was fabricated using 1.0 mm PMMA. Three 2 mm^3 neodymium magnets were incorporated onto the construct using a layer of adhesive film. A small motor was connected to the construct to induce automated movement of the magnets in a circular path beneath each HIA chamber.

Channel depths were calculated using Zeiss Axio A1 microscope fitted with a 5X objective.

Reagents

Dynabeads® MyOne™ Streptavidin C1 paramagnetic beads were purchased from Invitrogen (Carlsbad, CA). Salmonella enteric, serovar typhimurium LT2 DNA (700720D-5) was purchased from ATCC (Manassas, VA). Biotinylated oligonucleotides were purchased from Eurofins MWG Operon (Huntsville, AL). Potassium chloride and ethanol were purchased from Fisher Scientific (Fair Lawn, NJ). 2-Amino-2-(hydroxymethyl)- 1,3-propanediol (Trizma base, 99.9%) was purchased from Sigma (St. Louis, MO). All solutions were prepared in Nanopure water (Barnstead/Thermolyne, Dubuque, IA). SpeedSTAR™ polymerase, magnesium chloride and 10X PCR buffer, is available from Clontech Lab. (Mountain view, CA).

Conjugating Oligonucleotide Probes to Particles

Particles were prepared according to the manufacturer's protocol to produce stock particle concentration: 2 mg/mL. Final suspension buffer: 500 µL of 200 mM potassium chloride, 10 mM Trizma base, pH 7.5.

PCR

PCR was performed using the following cycling protocol: initial hold at 95 °C for 2 min followed by 32 cycles of 95 °C for 5 sec, 60 °C for 15 sec, and 72 °C for 20 sec, and then a final hold at 72 °C for 2 min. Final concentrations of reagents were, $MgCl^{2+}$ 3 mM, dNTP's 0.4 µM , 1x PCR buffer, polymerase 2.5 units, primers 2 µM. Non-integrated assays were then removed from the microdevice and the product was separated and detected using an Agilent 2100 Bioanalyzer (Agilent Technologies, Inc., Santa Clara, CA).

PCR primers and HIA probes

Forward PCR primer: 5'-AATTATCGCCACGTTCGGGCAA-3'
Forward HIA probe: 5'-[BioTEG] AATTATCGCCACGTTCGGGCAA-3'
Reverse PCR primer: 5'-TCGCACCGTCAAAGGAACC-3'
Reverse HIA probe: 5'-GGTTCCTTTGACGGTGCGA[BioTEG-Q]-3'

Image Analysis

For dye studies and HIA detection, images of the HIA chambers were collected using a T1i DSLR camera with MP-E 65 mm f/2.8 1−5× macro lens purchased from Canon U.S.A., Inc. (Lake Success, NY). Image processing was performed using Mathematica™ software.

Results and Discussion

Multiplexed IR-PCR

If HIA is to be an effective technique for sequence-specific DNA detection, it will either have to detect high copy number targets or rely on some form of DNA/RNA amplification to generate enough target for optically-detectable DNA-bead aggregation. It is in this respect that multiplexed PCR is important for specificity, and it is critical to include controls that minimize false negatives due to failure in amplification or sample preparation. With HIA, this facilitates simple interpretation of the results and immediate classification of the sample, via a visual side-by-side comparison with positive and negative controls.

To achieve multiplexed amplification in a microfluidic format that begins to address the potential for fully integrated analysis, four elliptical-shaped chambers, each having a volume of 2 μL, were symmetrically orientated within the 7 mm (diameter) focal spot of the halogen bulb (defined by the distance of chip positioned above the bulb); three are for PCR samples/controls, with the fourth used as a reference for temperature control (**Fig. 2A**). To evaluate temperature homogeneity across all PCR chambers, all chamber temperatures were measured simultaneously using independent thermocouples. The chamber-to-chamber variation in temperature was determined to be ± 2°C (data not shown). To test the effect of this variation on PCR performance, PCR specific for a 278 bp fragment of the *S. enterica* genome was carried out, and the PCR product generated in each chamber was analyzed by microchip electrophoresis using the Agilent Bioanalyzer (**Fig 2B**). Using the semi-quantitative capability of the Agilent Bioanalyzer, it was determined that ~3 ng (±0.3 ng) of the 278 bp fragment was produced in each of the microchip PCR reactions using 1 ng of pre-purified template DNA. With this defining comparable PCR results across all PCR chambers, it was concluded that the slight variation in temperature did not have a significant impact on PCR performance; therefore, three samples could be processed simultaneously on the device without a position-dependent bias.

Torque actuated pressure (TAP) system for reagent delivery

Following the completion of amplification, a reproducible volume of the PCR product must be transferred to the HIA chambers for sequence-specific detection. With the aim of avoiding the use of any form of external hardware for fluid flow control (to maintain low cost, portability and ease of use), we created a torque actuated pressure (TAP) system for fluid actuation. Using the turning of a 6-32" mechanical screw to force the elastomeric materials used to seal the device (septa and bio-film; described in following section) into the sample inlet, the PCR product is forced through the channel into the HIA detection chamber (**Fig. 3A**). For this, we fabricated a circular 1 mm deep cavity with a 1.33 mm radius, yielding a total inlet volume of 5.6 µL prior to any deformation of the elastomeric materials by the TAP. Dye studies were performed to verify the intra- and inter-device reproducibility of the TAP delivery system in precise mobilization and delivery of a desired volume of fluid. Blue dye (representing PCR reagents) was used to fill the inlet, PCR chamber and the channel to the valve, while yellow dye (representing HIA reagents) was used to fill the HIA detection chambers. As blue and yellow dyes mix as a result of the TAP activation, the hue resulting from the color change increases proportionally with the volume of blue dye added. A calibration curve was created by adding 3 µL of blue dye in 0.25 µL increments to the yellow dye, followed by image capture and processing[36]. The results from six separate trials showed that the TAP system was capable of reproducibly mobilizing 2 µL of fluid into the HIA reservoir with a variability of only 3.31% (**Fig. 3B**). This volume was attained through complete deformation of the elastomeric material by the TAP, which avoids any variability due to user-to-user differences in the degree to which the screw is turned. Accounting for unreacted master-mix in the channel upstream of the capillary valves, 1 µL of PCR product

was transferred into the HIA reservoir, which is the volume of PCR product previously determined to be optimal for the HIA assay[24].

The TAP reagent delivery system allows us to avoid limitations associated with the Wiebel et, al. TWIST valve on a PDMS device. First, reagent evaporation through permeation is observed in PDMS, which would prevent successful PCR; we avoid this by adopting a PMMA substrate. Additionally, the hysteresis of the PDMS prevents much of the available liquid in a compartment from being released with the TWIST valve; this is not an issue with our PMMA device. Finally, the fabrication process to incorporate the single-use screws into the PDMS device for the TWIST valve is labor-intensive, whereas the mutli-use TAP method utilizes simple one-time tapping of the PMMA manifold (which encases the microdevice) as the only extra 'fabrication' step required to incorporate the screws into the microfluidic system. This strategy of using a PMMA manifold to house the screws was also employed by Holcomb et al. to facilitate torque-actuated valving [37]; however, until now, this technique has not been demonstrated for fluid actuation and delivery.

Sealing and pressurization of the microdevice

The laser-ablated surface of the PMMA microdevice is rough, and thus prone to bubble formation[38]. Therefore, sealing and pressurization of the device was required to prevent bubble expansion, which would drive the PCR reagents out of the chamber during thermal cycling. In previous work, sealing and pressurization was achieved using biocompatible film and a PMMA manifold; however, this was applied to seal inlets with a radius of 0.5 mm and proved insufficient for our TAP inlets with nearly 3X the surface area (1.33 mm radius) (**Fig. 4A**) [38]. Therefore, an additional sealing component was required to prevent bubble expansion.

Additional pressure was applied with a septum (conventionally used to seal sample vials in capillary electrophoresis) placed above the inlets. The combination of bio-film, septa, and a PMMA manifold successfully minimized bubble expansion in the PCR chambers at 95 °C, allowing PCR to be performed successfully (**Fig. 4B**). The silicone composition of the septa prevented any sample loss through the bio-film, and was easily deformed with the application of the screw for fluid actuation. Importantly, due to the exceptional thermal stability of silicone, the elasticity of the septa is maintained even when exposed to the high temperatures required for PCR [39].

Capillary burst valves

In initial microdevice designs, the slight pressure that needed to be applied above the TAP inlets to assure sealing caused the premature movement of fluid through the PCR chamber, the microchannel, and into the HIA reservoirs. This can typically be avoided by applying even pressure across the device at all times; however, concurrently pressurizing the HIA reservoirs and PCR chambers would be challenging without the use of sophisticated pneumatic hardware. An alternative counter-pressurization scheme was used to immobilize the PCR reagents in the channel, based on a geometric capillary burst valve. The basis of this valve design stems from a previously reported 'fishbone valve'[40] involving the widening of a microchannel at a 90° angle to the direction of the flow; this creates the necessary surface tension to halt fluid flow. Such valves have been created in PMMA by laser-ablation using a rastering technique[32]. However, for effective valving, these require channels with a minimum dimension at the valve junction of 240 μm(w) x 600 μm (d), thus resulting in large dead-volumes (i.e., unreacted PCR reaction mix) that may be problematic for the downstream chemistry. Furthermore, our experience indicates that laser ablation systems can lack the necessary precision to connect vector and raster ablated

channels in the same plane (i.e., micron-scale resolution). For these reasons, we adapted the fishbone valve approach, using vector etching to create an opening perpendicular to the channel, reducing dead-volume and fabrication errors. Two burst valves in sequence were used, the second as a 'back-up' valve should the first valve be breached **(Fig. 5A,B)**. Notably, we never experience failure of the second valve with this device, while the failure rate of the first valve is ~5%. To minimize bubble formation caused by sharp corners in the microfluidic geometry, the valve was created with an oval shape and a depth of 170 μm – this was the minimal channel depth that could be reproducibly laser-ablated without channel collapse during thermal bonding (**Fig. 5C**). The valve was determined to burst at 0.4 PSI (2758 Pa), which is exceeded by the TAP to facilitate fluid movement to the detection chamber following PCR (data not shown).

HIA Detection

Once PCR amplification is completed, 1 μL volume of PCR product is mobilized to the HIA chamber for exposure to the oligonucleotide probe-adducted paramagnetic particles. Note that the HIA chambers were positioned 10 mm from the edge of the IR focal spot to minimize the effect of heating during PCR. As reported previously [24, 25, 41, 42], hybridization of the particle-bound probes to the amplified DNA in the presence of a rotating magnetic field (RMF) leads to particle aggregation. The single large bar magnet used previously was replaced with individual 2 mm^3 neodymium magnets positioned under each HIA detection chamber (**Fig. 6**). The magnets were encased in a machined PMMA holder connected to a small motor to induce automated movement of the magnets in a circular path beneath each HIA chamber. To avoid magnetic field cross-talk (magnet from one chamber affecting another chamber), the radius of rotation for each magnet required confinement to 3.5 mm underneath the 2.5 mm (radius) HIA well (**Fig. 6C**). By applying a magnetic field in this manner, the particle aggregation in the presence of target

sequence (or dispersion in the absence of target) was complete in 30 seconds, allowing for rapid, specific DNA detection.

Integrated amplification and detection of Salmonella enterica

To demonstrate functionality in an integrated format, however rudimentary, PCR amplification followed by direct bead aggregation detection was evaluated with the detection of *Salmonella enterica* in a sample. Using the same PCR protocol and reagents/primers used to generate the data in **Figure 2B (**and described in *Materials and Methods*), 32 cycles of IR-PCR was performed in only 34 minutes[36, 43]. In these analyses, the four chambers were utilized for thermocycling of positive control, negative control, test sample, and the reference chamber for temperature control (C3, C2, C1, and R1, respectively in **Fig. 2A**). In both the positive control and test sample chambers, 1 ng of pre-purified bacterial DNA was thermocycled. Following PCR, the HIA detection chambers were manually filled with HIA buffer and the oligonucleotide-bound particles. (Note that HIA reagents were not pre-loaded due to evaporation effects during PCR). TAP was initiated, moving any generated PCR products through the burst valves into the HIA chambers, where rotation of the mounted magnets at 150 rpm for 30 seconds enhanced the target-particle interaction. While aggregation was obvious to the naked eye, a custom algorithm was used to objectively evaluate the degree of aggregation (**Fig. 7**). With HIA, the greater the extent of aggregation, the larger the number of target molecules per unit volume in the sample. The software filters out the background, so only the aggregated particles are counted as 'pixels' (**Fig 7B**). This showed that the test sample had a 99 % Aggregation value that was comparable to the *Salmonella* positive control, while negative control resulted in a minimal HIA response (p value=0.002), confirming the presence of *Salmonella enterica* DNA in the sample (**Fig. 7C**).

These experiments represent the first instance of integrating PCR with HIA detection on a single microdevice.

Conclusions

This work describes key advances for the future integration of chemical processes on a single microdevice suitable for point of care NAT. We present the development of a novel PMMA microdevice that integrates two simple, inexpensive and novel analytical processes, IR-PCR and HIA detection. The multiplex format of the device allows for the inclusion of on-chip assay standards, enhancing the reliability of detection. Additionally, the capability for a visual read-out permits immediate interpretation of the results by the user and eliminates the need for additional instrumentation, which keeps costs low and portability high. Highly simplistic fluidic control was established, without the use of additional fabrication steps or peripheral instrumentation – this is key cost-efficiency in commercialization for rural or global health. We showed the functionality of the device with the successful detection of *Salmonella enterica* DNA in under 35 minutes. These results are a significant step to creating a functional, portable, easy-to-use POC microdevice for bacterial organisms. The versatility of this device will be utilized further, exploring targets of forensic and clinical value.

Acknowledgements

This research was supported by the National Institutes of Health. The authors gratefully acknowledge Agilent for providing the DNA 1000 kits used in this work.

References

1. A. Niemz, T. M. Ferguson and D. S. Boyle, *Trends in Biotechnology*, 2011, 29, 240-250.
2. C. A. Holland and F. L. Kiechle, *Current Opinion in Microbiology*, 2005, 8, 504-509.
3. C. Duarte, E. Salm, B. Dorvel, B. Reddy, Jr. and R. Bashir, *Biomed Microdevices*, 2013, DOI: 10.1007/s10544-013-9769-5, 1-10.
4. P. Yager, G. J. Domingo and J. Gerdes, *Annual Review of Biomedical Engineering*, 2008, 10, 107-144.
5. T. M.-H. Lee and I. M. Hsing, *Analytica Chimica Acta*, 2006, 556, 26-37.
6. P. Craw and W. Balachandran, *Lab on a Chip*, 2012, 12, 2469-2486.
7. L. Chen, A. Manz and P. J. R. Day, *Lab on a Chip*, 2007, 7, 1413-1423.
8. C. A. Baker, C. T. Duong, A. Grimley and M. G. Roper, *Bioanalysis*, 2009, 1, 967-975.
9. G. T. Walker, M. S. Fraiser, J. L. Schram, M. C. Little, J. G. Nadeau and D. P. Malinowski, *Nucleic acids research*, 1992, 20, 1691-1696.
10. J. Compton, *Nature*, 1991, 350, 91-92.
11. A. Fire and S. Q. Xu, *Proceedings of the National Academy of Sciences*, 1995, 92, 4641-4645.
12. C. Zhang and D. Xing, *Nucleic acids research*, 2007, 35, 4223-4237.
13. Y. Zhang and P. Ozdemir, *Analytica Chimica Acta*, 2009, 638, 115-125.
14. S. Park, Y. Zhang, S. Lin, T.-H. Wang and S. Yang, *Biotechnology Advances*, 2011, 29, 830-839.
15. C. J. Easley, J. M. Karlinsey and J. P. Landers, *Lab on a Chip*, 2006, 6, 601-610.
16. M. G. Roper, C. J. Easley, L. A. Legendre, J. A. C. Humphrey and J. P. Landers, *Analytical Chemistry*, 2007, 79, 1294-1300.

17. D. Le Roux, B. E. Root, J. A. Hickey, O. N. Scott, A. Tsuei, J. Li, D. J. Saul, L. Chassagne, J. P. Landers and P. de Mazancourt, *Lab Chip*, 2014, 14, 4415-4425.

18. M. A. Burns, B. N. Johnson, S. N. Brahmasandra, K. Handique, J. R. Webster, M. Krishnan, T. S. Sammarco, P. M. Man, D. Jones, D. Heldsinger, C. H. Mastrangelo and D. T. Burke, *Science*, 1998, 282, 484-487.

19. E. T. Lagally, C. A. Emrich and R. A. Mathies, *Lab on a Chip*, 2001, 1, 102-107.

20. D. Trau, T. M. Lee, A. I. Lao, R. Lenigk, I. M. Hsing, N. Y. Ip, M. C. Carles and N. J. Sucher, *Anal Chem*, 2002, 74, 3168-3173.

21. R. C. Anderson, X. Su, G. J. Bogdan and J. Fenton, *Nucleic acids research*, 2000, 28, e60.

22. M. A. Northrup, B. Benett, D. Hadley, P. Landre, S. Lehew, J. Richards and P. Stratton, *Anal Chem*, 1998, 70, 918-922.

23. J. G. Lee, K. H. Cheong, N. Huh, S. Kim, J. W. Choi and C. Ko, *Lab Chip*, 2006, 6, 886-895.

24. D. C. Leslie, J. Li, B. C. Strachan, M. R. Begley, D. Finkler, L. A. L. Bazydlo, N. S. Barker, D. M. Haverstick, M. Utz and J. P. Landers, *Journal of the American Chemical Society*, 2012, 134, 5689-5696.

25. B. C. Strachan, H. S. Sloane, J. C. Lee, D. C. Leslie and J. P. Landers, *Analyst*, 2015, 140, 2008-2015.

26. K. Xu, M. R. Begley and J. P. Landers, *Lab on a Chip*, 2015, 15, 867-876.

27. K. Iwai, K. C. Shih, X. Lin, T. A. Brubaker, R. D. Sochol and L. Lin, *Lab on a Chip*, 2014, 14, 3790-3799.

28. W. Li, T. Chen, Z. Chen, P. Fei, Z. Yu, Y. Pang and Y. Huang, *Lab on a Chip*, 2012, 12, 1587-1590.

29. D. B. Weibel, M. Kruithof, S. Potenta, S. K. Sia, A. Lee and G. M. Whitesides, *Analytical Chemistry*, 2005, 77, 4726-4733.

30. M. A. Unger, H.-P. Chou, T. Thorsen, A. Scherer and S. R. Quake, *Science*, 2000, 288, 113-116.

31. J. Melin and S. R. Quake, *Annu Rev Biophys Biomol Struct*, 2007, 36, 213-231.

32. M. I. Mohammed, E. Abraham and M. P. Y. Desmulliez, *Journal of Micromechanics and Microengineering*, 2013, 23, 035034.

33. A. L. Brogger, D. Kwasny, F. G. Bosco, A. Silahtaroglu, Z. Tumer, A. Boisen and W. E. Svendsen, *Lab on a Chip*, 2012, 12, 4628-4634.

34. A. S. Patterson, D. M. Heithoff, B. S. Ferguson, H. T. Soh, M. J. Mahan and K. W. Plaxco, *Appl Environ Microbiol*, 2013, 79, 2302-2311.

35. Y. C. K. Yi Sun, Nam-Trung Nguyen, *Journal of Micromechanics and Microengineering*, 2006, 16.

36. J. A. Lounsbury, A. Karlsson, D. C. Miranian, S. M. Cronk, D. A. Nelson, J. Li, D. M. Haverstick, P. Kinnon, D. J. Saul and J. P. Landers, *Lab on a Chip*, 2013, 13, 1384-1393.

37. R. E. Holcomb, L. J. Mason, K. F. Reardon, D. M. Cropek and C. S. Henry, *Anal Bioanal Chem*, 2011, 400, 245-253.

38. J. A. Lounsbury, B. L. Poe, M. Do and J. P. Landers, *Journal of Micromechanics and Microengineering*, 2012, 22, 085006.

39. C. L. Joost, O. Wouter, H. V. Peter and B. Piet, *Journal of Micromechanics and Microengineering*, 1996, 6, 52.

40. C. Lu, Y. Xie, Y. Yang, M. M. C. Cheng, C.-G. Koh, Y. Bai, L. J. Lee and Y.-J. Juang, *Analytical Chemistry*, 2006, 79, 994-1001.

41. D. A. Nelson, Strachan, Briony C., Sloane, Hillary S., Li, Jingy, Landers, James P., *Analytica Chimica Acta*, 2014, Accepted, Jan 2014.

42. H. S. Sloane, K. A. Kelly and J. P. Landers, *Anal Chem*, 2015, DOI: 10.1021/acs.analchem.5b01876.

43. J. A. Lounsbury, N. Coult, D. C. Miranian, S. M. Cronk, D. M. Haverstick, P. Kinnon, D. J. Saul and J. P. Landers, *Forensic Science International: Genetics*, 2012, 6, 607-615.

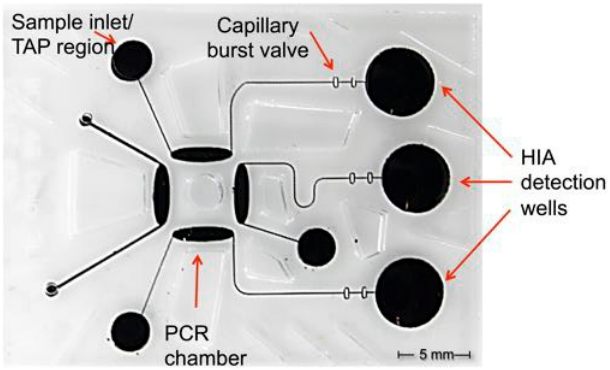

Figure 1: Image of the fabricated PMMA multiplex integrated microdevice, filled with black dye for feature visualization. Highlighted are the four main domains of the device: PCR, valving (burst valve), sample inlet (which is depressed when fluid is mobilized with TAP following PCR) and HIA detection region. Additional features surrounding the primary architecture of the microdevice are 'air pockets,' created to reduce the thermal mass of the device and to aid in bonding during device fabrication.

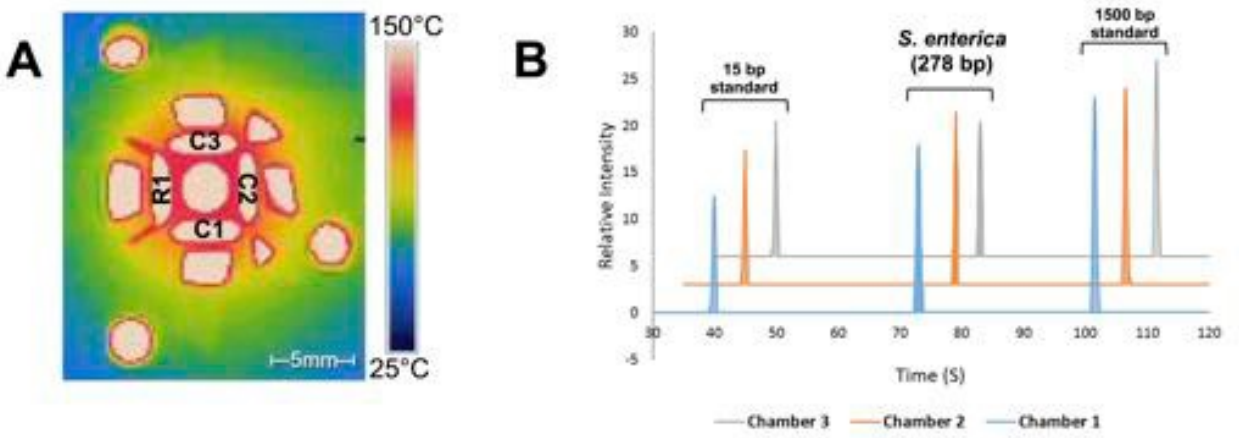

Figure 2: Design and results of multiplex PCR with a halogen bulb. A) IR camera image of the top layer of the microdevice during thermocycling. PCR chamber are in a symmetrical arrangement around the focal spot of the halogen bulb. The 7 mm diameter represents the hottest section, providing fast heating rates. Each PCR chamber is sized to scale. B) Electropherograms of multiplex IR-PCR amplification of a 278 bp region of Salmonella enterica. Lightly shaded peaks are the 15 and 1500 bp markers, respectively. Each chamber position corresponds to those in A.

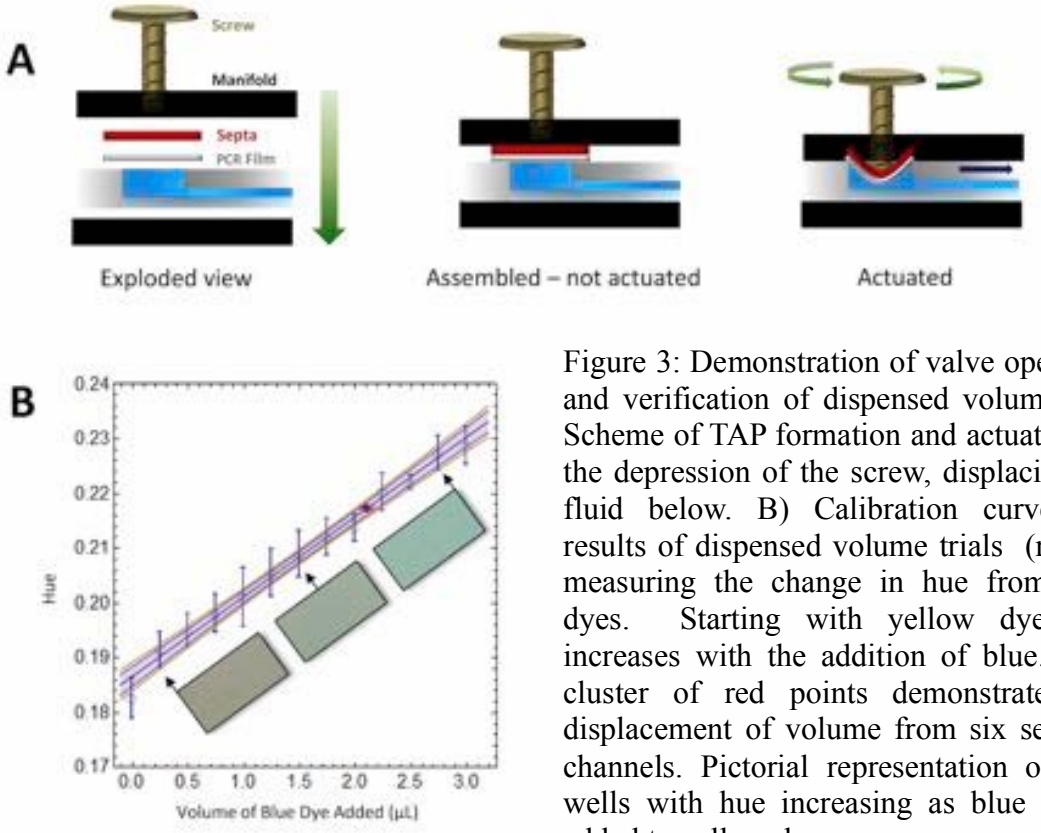

Figure 3: Demonstration of valve operation and verification of dispensed volume. A) Scheme of TAP formation and actuation by the depression of the screw, displacing the fluid below. B) Calibration curve and results of dispensed volume trials (red) of measuring the change in hue from food dyes. Starting with yellow dye, hue increases with the addition of blue. The cluster of red points demonstrates the displacement of volume from six separate channels. Pictorial representation of HIA wells with hue increasing as blue dye is added to yellow dye.

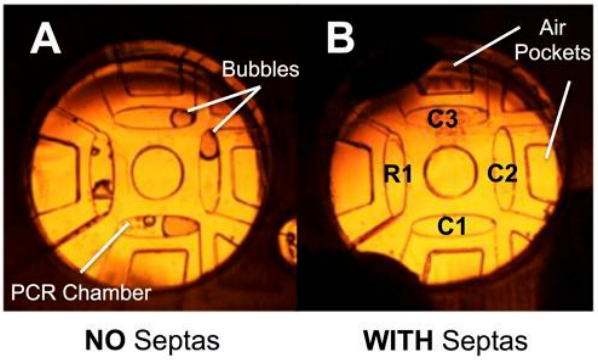

Figure 4: Top-view photographs of the PCR chambers at 95 °C. A) Bubbles are seen in the PCR chambers when no septa is applied. B) No bubbles are visible to the naked eye with the addition of a septa for additional pressurization. HIA chambers are positioned to the right of the chambers.

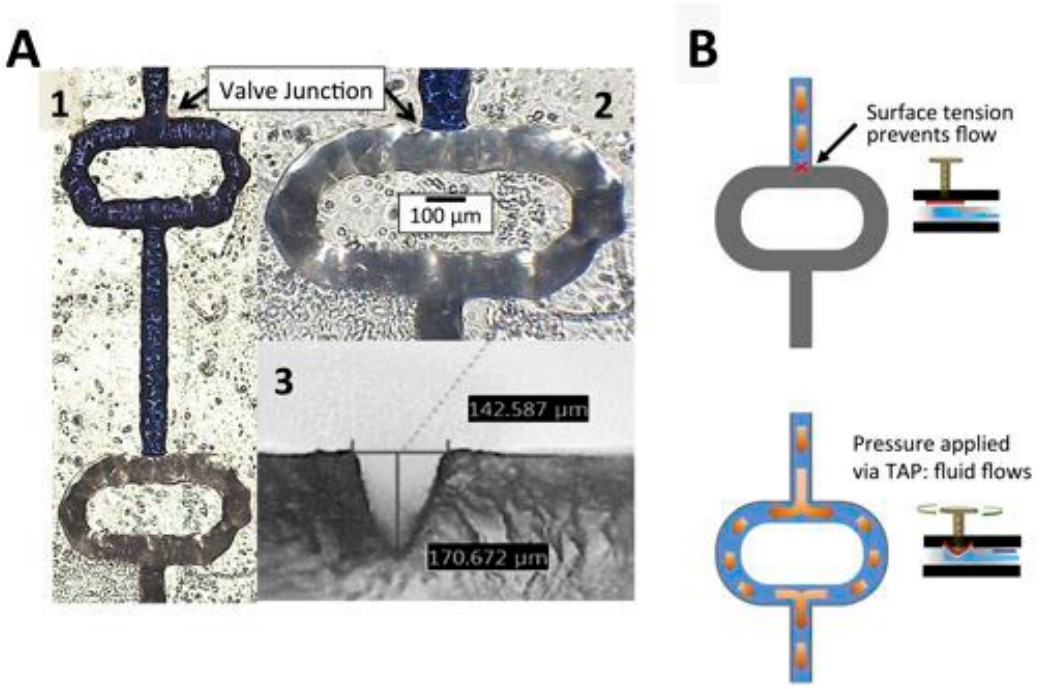

Figure 5: A) Microscope images of the capillary valve and channel shape and depth in PMMA. A1) Image demonstrating that if the first valve is broken, the second valve will hold. A2) Close-up of the valve preventing fluid flow through surface tension. A3) Cross-sectional view of the channel architecture in the device. All channels are ~150 µm wide and ~170 µm deep. B) Schematic demonstrating the principles of fluidic control using the capillary valve and TAP system.

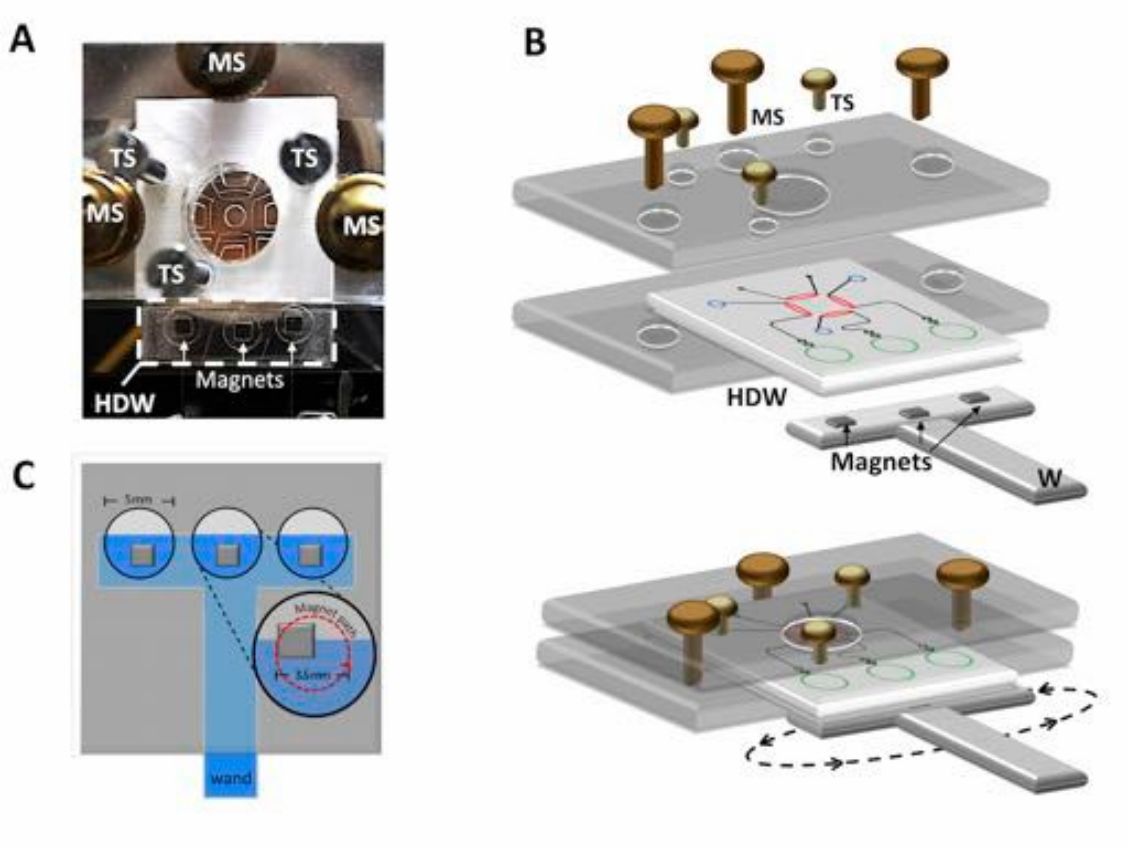

Figure 6: Placement of discrete individual magnetic field for HIA detection. A) Top-view photograph of the HIA chambers with individual magnets below. B) Scheme of microdevice held in manifold following pressurization with placement of the magnets held in a PMMA cross-T. C) Scheme of 2 mm^2 magnets rotating within a 3.5 mm diameter. MS, manifold screw; TS, TAP screw; HDW, HIA detection well; W, rotating magnetic wand.

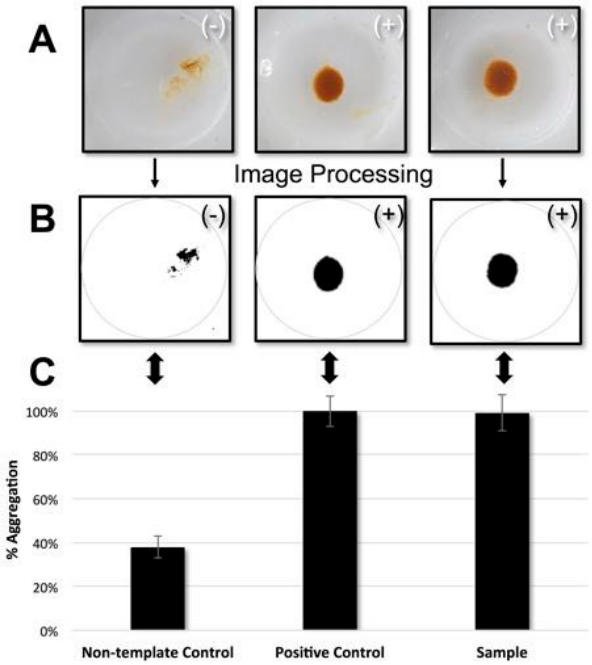

Figure 7: Results from an integrated analysis for the detection of salmonella enterica. A) Images of HIA well showing the extent of aggregation after exposure to a RMF for 30 seconds. B) Images showing algorithmic conversion into the pixelized image that provides semi-quantitative information. C) Bar graph generated from algorithm analysis of the aggregation in (B). For n=3, % CV for Non-template Control, Positive Control and Sample were 5, 9 and 8% respectively.